JOURNAL OF GEOPHYSICAL RESEARCH, VOL. 101, NO. C7, PAGES 16,345–16,359, JULY 15, 1996

Responses of the tropical Pacific to wind forcing as observed by spaceborne sensors and simulated by an ocean general circulation model

W. Timothy Liu and Wenqing Tang
Jet Propulsion Laboratory, California Institute of Technology, Pasadena

Robert Atlas
Laboratory for Atmospheres, NASA Goddard Space Flight Center, Greenbelt, Maryland

Abstract. In this study, satellite observations, in situ measurements, and model simulations are combined to assess the oceanic response to surface wind forcing in the equatorial Pacific. The surface wind fields derived from observations by the spaceborne special sensor microwave imager (SSM/I) and from the operational products of the European Centre for Medium-Range Weather Forecasts (ECMWF) are compared. When SSM/I winds are used to force a primitive-equation ocean general circulation model (OGCM), they produce 3°C more surface cooling than ECMWF winds for the eastern equatorial Pacific during the cool phase of an El Niño–Southern Oscillation event. The stronger cooling by SSM/I winds is in good agreement with measurements at the moored buoys and observations by the advanced very high resolution radiometer, indicating that SSM/I winds are superior to ECMWF winds in forcing the tropical ocean. In comparison with measurements from buoys, tide gauges, and the Geosat altimeter, the OGCM simulates the temporal variations of temperature, steric, and sea level changes with reasonable realism when forced with the satellite winds. There are discrepancies between model simulations and observations that are common to both wind forcing fields, one of which is the simulation of zonal currents; they could be attributed to model deficiencies. By examining model simulations under two winds, vertical heat advection and uplifting of the thermocline are found to be the dominant factors in the anomalous cooling of the ocean mixed layer.

1. Introduction

The combination of satellite observations and a numerical ocean circulation model has been promoted since the 1970s as a potentially powerful tool to study the traditionally undersampled ocean, particularly to understand the basin-wide oceanic responses to atmospheric forcing. With the accumulation of data from operational sensors such as the advanced very high resolution radiometer (AVHRR) and the special sensor microwave imager (SSM/I), with the recent launching of research satellites such as Geosat, TOPEX/POSEIDON, and ERS 1, and with the fast-improving accessibility of affordable supercomputer time to run the ocean general circulation model (OGCM), the potential is being realized.

Ocean circulation is driven by surface wind stress. Present wind data over the ocean are inadequate; they are primarily observations from volunteer ships which cover only limited regions at irregular time intervals. In the past, only climatological wind fields derived from averaging ship observations made over a long period of time were available to force basin-wide ocean models; such climatological winds are without much of the natural variability. Operational numerical weather prediction (NWP) models and spaceborne sensors have the potential of providing wind fields that would excite more realistic oceanic responses. The responses to these forcings, in turn, would differentiate the quality of these wind fields and might reveal the deficiency of model physics. With realistic surface forcing and reasonably accurate model physics the model results should reveal the physical mechanisms by which the ocean responds to surface forcing; such mechanisms are not clearly discerned by spaceborne sensors which cannot probe ocean depth and are not sufficiently resolved by sparse in situ measurements.

The equatorial Pacific, where wind forcing is most directly felt and where the interannual signal caused by El Niño–Southern Oscillation (ENSO) is large, is the selected region of this study. This region is also blessed with the Tropical Atmosphere and Ocean (TAO) buoy array and island tide gauges, all of which are part of the monitoring system of the Tropical Oceans and Global Atmosphere (TOGA) Program; the buoys and tide gauges provide valuable in situ measurements that are used to validate satellite data and model simulations. The study covers a 3-year period, from July 1987 to June 1990. The period was selected because of the availability of SSM/I wind velocity. It includes part of the warm phase and the entire cool phase of the 1987–1988 ENSO event. While the reference to the warm phase as El Niño has been generally accepted, the naming of the cold phase is controversial; El Viejo and La Niña have been used.

Wind fields from the NWP models of the European Center for Medium-Range Weather Forecasts (ECMWF) and derived

Paper number 96JC01347.
0148-0227/96/96JC-01347$09.00

from SSM/I observations, in various forms, have been evaluated through direct comparisons in previous studies [e.g., *Busalacchi et al.*, 1993; *Halpern et al.*, 1994]. In this study the two wind fields are evaluated mainly through the responses they generate from a primitive-equation OGCM. Such an approach was initiated by *Tang and Liu* [1992], using a shorter period of data, with an early version of the OGCM, and before the availability of in situ measurements to serve as independent standards. The sea surface temperature (SST) and sea level changes simulated by the OGCM when forced by these two wind fields will be compared with those derived from the AVHRR and the Geosat altimeter observations. These parameters and other diagnostics will also be compared with measurements at moored buoys. The OGCM and the data used are described in section 2 and section 3, respectively. Direct comparisons of the two wind fields are given in section 4. The model simulations will be examined in comparisons with in situ measurements and satellite observations in section 5. In section 6 the upper ocean heat budget will be discussed in an attempt to shed light on the dominant mechanism by which surface temperature is changed by wind forcing. The conclusion is given in section 7.

2. Ocean General Circulation Model

The Modular Ocean Model (MOM) developed at the Geophysical Fluid Dynamics Laboratory [*Bryan and Cox*, 1972] was used in this study. It is an improved and more general version of the model used by *Tang and Liu* [1992]. The model uses Boussinesq and hydrostatic approximations. The vertical mixing coefficient is formulated as an empirical function of the Richardson number [*Philander et al.*, 1987]. The horizontal domain is chosen to cover the Pacific Ocean from 30°S to 50°N and from 130°E to 70°W. Following the tradition for applying this model, a no-slip condition is applied at the lateral wall. Near the north and south boundaries the temperature and salinity are relaxed to the climatological seasonal values [*Levitus*, 1982], and no flux of heat or salt is allowed on the east and west boundaries. The longitudinal resolution is 1°, and the latitudinal resolution is 1/3° within the equatorial band of 10° from the equator but increases to 2.5° at the north and south boundaries. The model has constant depth of 4149 m, with 27 levels. The model time step is 1 hour.

The initial conditions are the January climatological temperature and salinity, with no current. The downwelling insolation is taken to be 242 W/m^2 within 20° from the equator and to decrease linearly to 151 W/m^2 at 45° latitude. The outgoing longwave radiation has a constant value of 56 W/m^2. The sensible and latent heat fluxes are computed through the bulk aerodynamic formula, using model-simulated sea surface temperature and climatological surface air temperature [*Oort et al.*, 1987]. The transfer coefficients of heat and water vapor are assumed to be 0.0012. The relative humidity is assumed to be 80%.

The OGCM was run for a 3.5-year period, driven by climatological wind stress [*Hellerman and Rosenstein*, 1983]. After this 3.5-year spin-up the model reaches a quasi-equilibrium seasonal cycle. Then three parallel runs were started by applying two different wind stress fields (as discussed in section 3) and by continuing the run with climatological forcing as the control, covering 3 years, starting in July 1987. The surface heat flux remained unchanged. Output parameters were averaged every 3 days in this study.

The ocean temperature and salinity profiles produced by the OGCM are used to compute the steric level, or dynamic height h; the computation involves an integration of the specific volume anomaly δ from a reference level h_r to the surface:

$$h = \int_0^{h_r} \delta \, dz$$

The specific volume anomaly δ is defined as

$$\delta = \alpha(S, T, z) - \alpha(35, 0, z)$$

where the specific volume α is the invert of density and is a function of depth z, salinity in practical salinity units (psu) (S), and temperature in degrees Celsius (T).

For the surface the model uses a rigid-lid approximation and simulates the pressure gradient. To compute the sea level H, we first reconstruct the surface pressure P field from the gradient by using an inversion technique, with the constraint that P averaged over the model domain is equal to zero at each inversion step. The sea level is then computed from the hydrostatic relation

$$P = \rho g H$$

where ρ is the surface density and g is the acceleration due to gravity.

3. Data

Three sets of wind fields are used to force the model. The first set consists of the wind stress fields computed by *Hellerman and Rosenstein* [1983] from 116 years (1870–1986) of wind reports from volunteer ships, using *Bunker*'s [1976] drag coefficients, which increase with wind speed and atmospheric instability. This wind climatology is used in spinning up the model and as a control run. The second set consists of wind velocity field at 10-m height, taken from the ECMWF/TOGA Level III data set. This is the noninitialized, analyzed data field produced by the NWP center at the ECMWF [*Bengtsson et al.*, 1982]. This set of data is hereafter referred as "ECMWF winds." The third set is based on wind speed measured by the SSM/I [*Wentz*, 1992]. The wind direction is determined by a variational method using all available data [*Atlas et al.*, 1991, 1993]. This set of data is hereafter referred to as "SSM/I winds." Three years of data, from July 1987 to June 1990, from the latter two data sets are used in this study.

In computing wind stress from ECMWF and SSMI winds a variable drag coefficient that accounts for the transition from rough flow (high wind) to smooth flow (low wind) and for variation in the height of measurements is used; neutral stability is assumed [*Liu et al.*, 1979]. The ECMWF provides, as a standard product, surface wind at 1000 mbar derived from the initialized analysis, and this product was used by *Busalacchi et al.* [1993] to compare with the first year of SSM/I winds. The uncertainty in the altitude of the isobaric surface, however, poses a serious problem for converting the wind vector into momentum flux, or wind stress, because the wind shear near the surface could be large. The ECMWF/TOGA Level III archive was produced partly to alleviate this difficulty. The climatological wind is monthly at a 2° latitude by 2° longitude spatial resolution. The SSM/I wind has 6 hourly and 2° latitude by 2.5° longitude resolutions, while the ECMWF wind has semidaily and 2.5° by 2.5° resolutions. The wind data are lin-

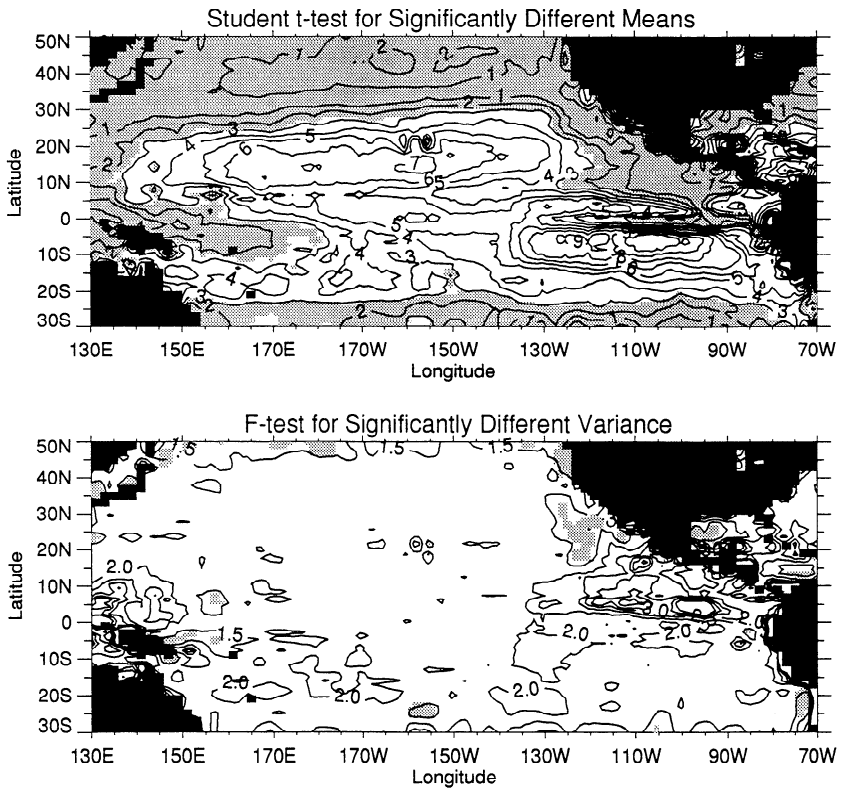

Figure 1. Distribution of the absolute value (top) Student's t, which is the mean difference between special sensor microwave imager (SSM/I) and European Centre for Medium-Range Weather Forecasts (ECMWF) zonal wind stresses divided by the standard error, and (bottom) F function, which is the ratio of the variances of the two zonal wind stresses. Areas where the values of Student's t and F function have more than 1% probability to come by pure chance from wind stresses of equal means and variances are stippled.

early interpolated to the time step (hourly) and to the spatial grid of the OGCM.

The SST is taken from 1° latitude by 1° longitude and weekly maps produced through optimal interpolation using AVHRR data blended with in situ data [*Reynolds and Smith*, 1994], and this data set is hereafter referred to as the "AVHRR SST." Sea level residues from the Geosat altimeter start from the geophysical data records with environmental corrections [*Cheney et al.*, 1987]. Subsequent processing, including orbit-error removal, was described by *Zlotnicki et al.* [1989]. The data were made available to us as 2.5° latitude by 2.5° longitude maps every 15 days, and this data set is referred to as "Geosat sea level." Daily surface wind vectors and ocean temperatures measured at the TOGA TAO moorings [*Hayes et al.*, 1991] are also used for comparison. The surface winds at these moorings are measured at 4 m and are converted to surface stress with the model of *Liu et al.* [1979], as described. Daily sea level data from tide gauges of the TOGA Pacific sea level network [*Wyrtki et al.*, 1988] were also used in the comparison.

4. Zonal Wind Stress Comparison

The means and variances of the SSM/I and ECMWF winds for the 3-year period have similar geographical distributions but different strengths. To find out the statistical significance of the differences between the means and the variances, standard Student's t and F tests are performed [*Press et al.*, 1989], and the results are shown in Figure 1. Large and significant differences of the mean are found between 25°N and 25°S in the Pacific Ocean, except in an area roughly within 200 km from the American coast north of the 10°N, in an area west of 170°E between the equator and 10°S, and in a narrow zonal belt along the equator between 80°W and 120°W. The mean differences are large along two zonal belts centered at 15°N and 5°S. We have no good explanation on the distribution. Large and significant values of F are found in the eastern and western Pacific within 20° latitude north of the equator.

While the underlying cause for the distributions of the normalized mean difference and ratio of variance is not apparent, the temporal characteristics of the differences are revealed in time series comparisons at selected off-equatorial locations in Figure 2 and equatorial locations in Plate 1. The 12 hourly data are passed through a 10-day running mean filter to give graphic clarity in the figures. In Figure 2 the temporal variations are dominated by periods of strong wind separated by quiescence periods of low wind. The strong winds are easterly, except at 5°N and 80°W. The two sets of wind appear to roughly agree during the quiescence periods, but SSM/I winds indicate much more strength at the peak of the strong wind events. Unfortunately, there are no high-quality in situ wind measurements to evaluate the two sets of winds at these off-equatorial locations where the differences are relatively large.

There are in situ wind measurements from the TAO moored buoys along the equator, but the mean differences between SSM/I and ECMWF winds are relatively small at these locations. The buoy measurements and the climatological annual cycles are included in Plate 1. The differences in intensity

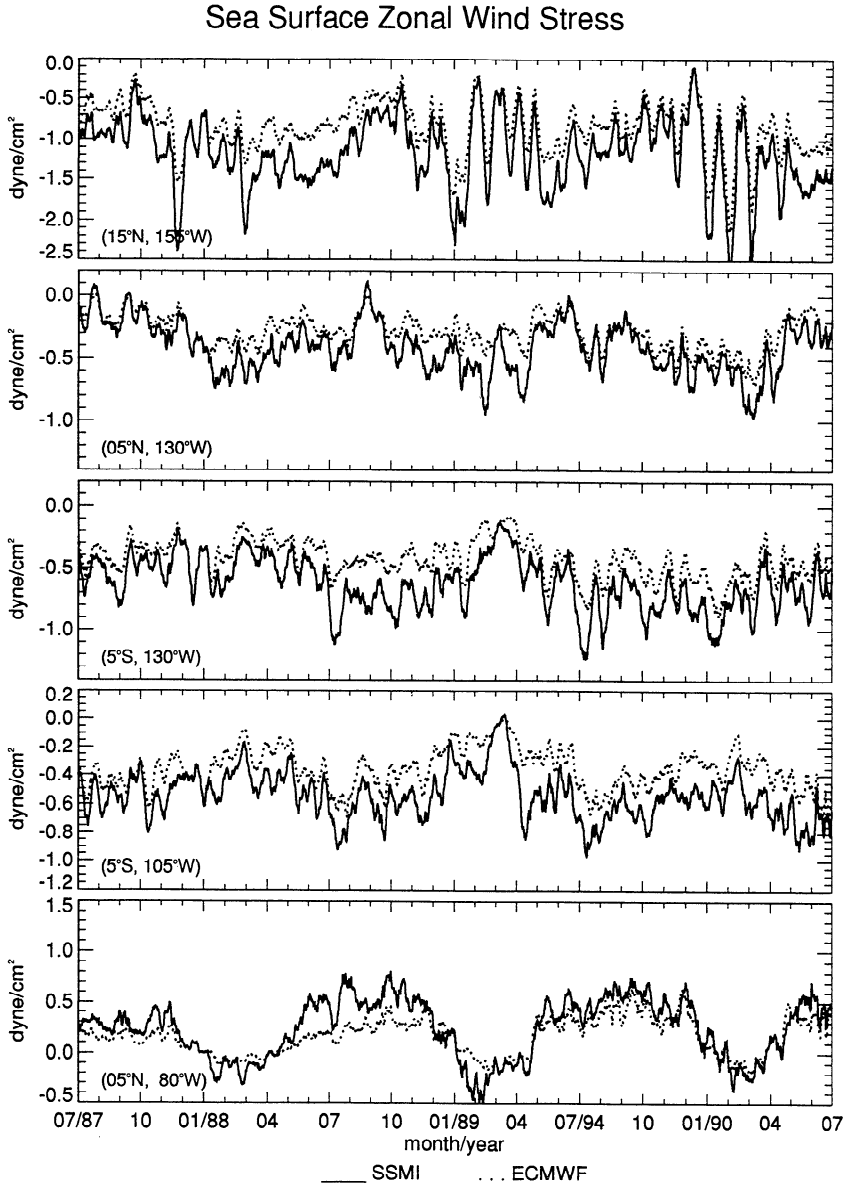

Figure 2. Comparison of the zonal component of surface wind stress derived from SSM/I observations and from ECMWF analysis at selected locations (latitudes and longitudes are indicated in the figure).

during wind events are still present. At 165°E, buoy measurements at latitudes 2°N, 0°, and 2°S are averaged together because there are large data gaps at each latitude, but for the other three longitudes, only measurements at the equator are used. The climatological annual cycles shown in Plate 1 are compiled from buoy data; the length of the data sets varies from approximately 6 years at 170°W to 11 years at 140°W. The annual cycle is prominent at 110°W and 140°W but becomes less conspicuous at 170°W and 165°E. Both SSM/I and ECMWF winds show eastward anomalies during the warm phase of ENSO in 1987 at all three stations east of the dateline and westward anomalies during the cold phase of ENSO in 1988 at 165°E and 170°W.

Using 3 years of SSM/I and ECMWF data coincident with the daily buoy data, correlation coefficients are computed. The correlations between SSM/I and ECMWF zonal wind stresses are significantly higher than the correlations between buoy measurements and either SSM/I or ECMWF data at all four locations. The correlation coefficients between SSM/I and ECMWF wind are 0.96, 0.94, 0.96, and 0.74 at buoy locations from west to east. The correlation coefficients between SSM/I and buoy data are the same as between ECMWF and buoys to the first decimal; they are 0.6, 0.6, 0.5, and 0.4, respectively. The results underscore the problem with the traditional method of evaluating winds averaged over satellite footprint or over model grid size by comparison with point measurement (at buoy). The difficulty in matching temporal and spatial coverages and the limited availability of accurate standards illuminate the need for the comparison of the oceanic responses forced by difference winds stresses presented in section 5.

5. Comparing Model Simulation With In Situ Measurements

5.1. Surface Temperature

To clarify the difference in temperature response to SSM/I and ECMWF wind forcing, time series of the first-level (5-m)

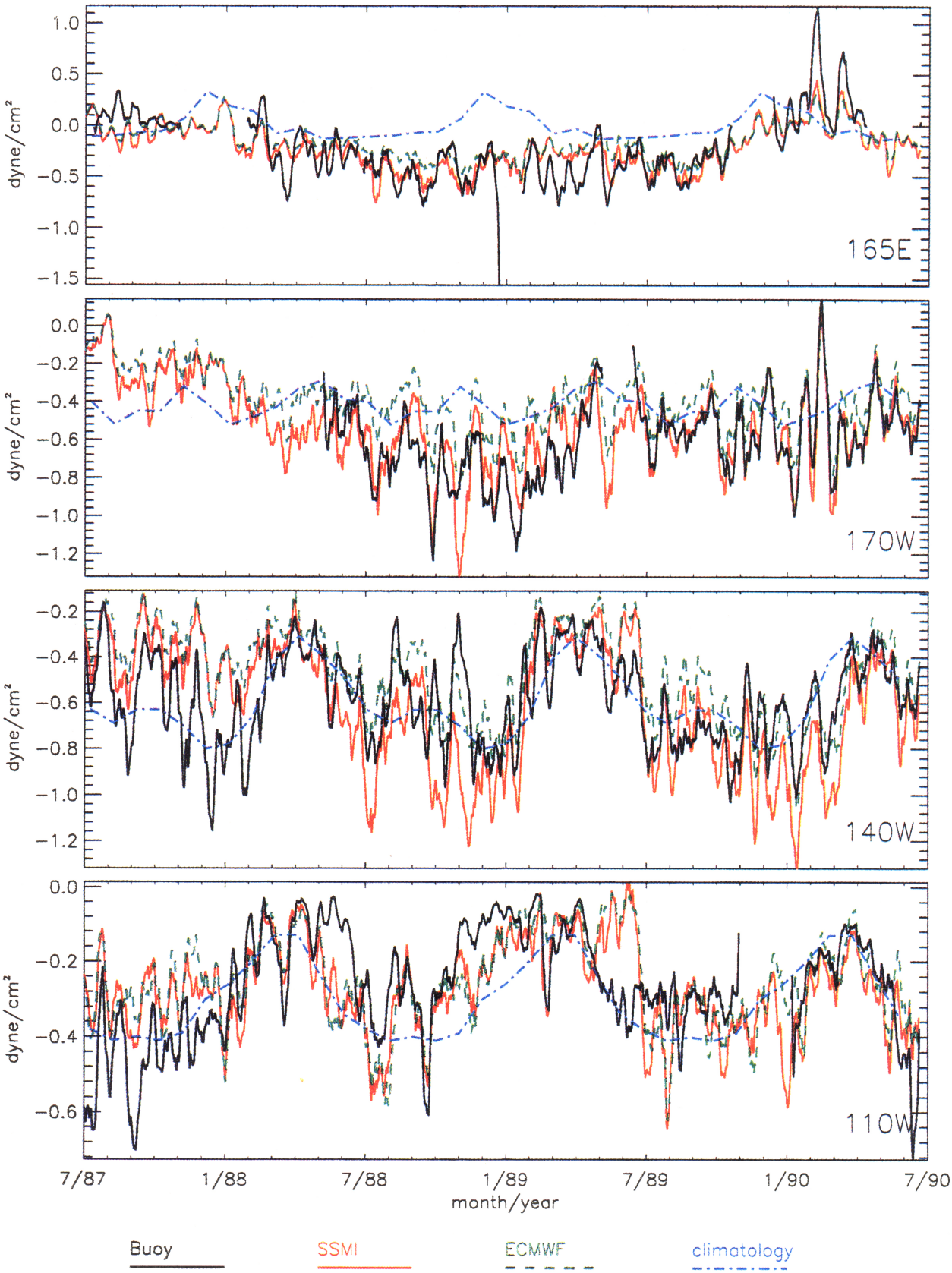

Plate 1. Same as Figure 2, but at four selected locations along the equator and with additional comparison with buoy measurements (longitudes are indicated in the plate). The climatological annual cycle compiled from buoy data is also shown.

temperature produced by the OGCM when forced by various winds are compared with the AVHRR SST and measurements made at equatorial buoys (Plate 2). Sufficiently continuous SST measurements are available only at three equatorial moorings (110°W, 140°W, and 165°E). The climatological annual cycle is compiled from 7 years (July 1983 to June 1990) of the AVHRR SST. For all four locations the model starts at temperatures that resulted from climatological winds and are close to climatological SST, which is lower than the observations at locations east of the dateline. When more realistic winds from the ECMWF and SSM/I are applied, the model temperature adjusts to observed values at locations after a few months and remains in rough agreement with observations extending through the warm phase of ENSO. Starting in March 1988, the observed temperature dropped sharply to below climatological values; the drop is more than 7°C at 110°W. The warm and cold ocean temperature anomalies during the 1987–1988 ENSO event have been described by *McPhaden and Hayes* [1990] and others, using data from TAO buoys. When the model is forced by SSM/I winds, the model temperature drops by an amount similar to the observed temperature drops (from AVHRR and buoy data), but the model temperature resulting from ECMWF wind forcing remains at climatological values at locations east of the dateline. The difference in temperatures caused by ECMWF and SSM/I forcing exceeds 3°C in October 1988 at all three locations east of the dateline. Similar differences in SST simulations were observed by *Tang and Liu* [1992].

East of the dateline, the temperatures start to rise around November 1988 and approach climatological values in early 1989, but the model temperatures that result from ECMWF winds are always higher than those resulting from SSM/I winds. For 1990 at the stations east of the dateline, both model simulations indicate cold anomalies not present in the observations. At 165°E the differences between model simulations are relatively small, and there is general agreement between the model simulation and the observations, except during the periods June–December 1989 and May–June 1990; the reason for these discrepancies is unclear.

The maximum differences in mean zonal wind stress are off the equator and the coast, as shown in Figure 1, but the largest differences in SST response (not shown) are bounded to the eastern equatorial Pacific and the American coast. At the three locations east of the dateline the SST simulations forced by ECMWF winds have significantly larger deviations from observations by AVHRR than simulations forced by SSM/I winds, in both mean and variance, as shown in Table 1. Similarly, using SSM/I wind also significantly improves the correlation coefficient between SST simulations and observations. The statistics in Table 1 are computed from 363 pairs of data in 3 years at 3-day resolution. The probabilities that the reduction in mean and variance of the "errors" (deviation from observations) arises by pure chance from "errors" distributions with equal means and variances are less than 1% for all locations, except the 10% value for variance at 110°W. The probability that the improvement of correlation by SSM/I winds arises by pure chance from two distributions with equal correlations is less than 1% at 140°W and 130°W and increases only to 3% at 110°W. A similar conclusion can be drawn with buoy surface temperature replacing AVHRR data.

The close agreement between AVHRR and buoy SST is an indication of the high quality of observations. The most striking result shown in Plate 2 is that the SSM/I wind produces a more realistic anomalous surface cooling in 1988 for the cool phase of ENSO than the ECMWF wind does. Another implication is on the robustness of the OGCM. All the correlation coefficients between model simulations and observations are significant; there is less than 1% chance that the correlations are results of chance. Overall, the model simulates the temporal variability of SST when forced by winds with reasonable realistic temporal signal. There are periods when model simulations are different from observations under both wind forcings; the differences are likely to be caused by the deficiency of model physics or the lack of realistic thermal and hydrologic forcing.

5.2. Steric Level

The temperature difference should be reflected in density structure, and the wind-forced temperature response is not likely be confined to the surface. The depth-integrated density response to different wind forcing is examined in Figure 3, where the variations of steric level (dynamic height) between 300 m and the surface at the four buoy locations are shown. The temporal variations of steric levels are roughly opposite to those of the mixed-layer depths (not shown). The most prominent feature is the extremely low steric level in the eastern Pacific during the cool phase of the ENSO in 1988. At 170°W, observations from buoy are not available most of the time. For the cold phase, SSM/I winds forced a lower steric level and therefore, in closer agreement with observations, at both 140°W and 110°W than ECMWF winds did. This is reflected in the significantly smaller mean deviations of the simulation from observations when forced by SSM/I winds than from the simulation forced by ECMWF winds, as shown in Table 2. However, the variances are not significantly different. The correlation coefficient between all model simulations and observations is significant at 99% level, indicating that the model is capable of simulating the temporal variation of the steric change. The simulations that resulted from SSM/I and ECMWF winds do not produce significantly different correlation coefficients with observations, as indicated by the large values of the significance in Table 2.

For 1987 the buoy data are more than 0.1 m lower than the model data. For 110°W the buoy data are lower than the model results for the entire period. Salinity profiles are used to compute steric level, but the salinity measurements at the buoys and salinity field produced by the model have not been vigorously validated in the past.

5.3. Sea Level

The change of sea level, of course, reflects both the steric change and deep current [*Gill and Niiler*, 1973]. The time series of the sea level computed from model data (with the 3-year mean removed) are compared with tide gauge and altimeter data for six near-equatorial (between 2°N and 4°S) tide gauge stations across the Pacific in Plate 3. The determination of absolute sea level from the tide gauge and altimeter data is difficult because of the lack of a reference. In Plate 3 the mean of the time series for each location is removed to ensure that the data sets are referenced to the same mean surface. Essentially, each data time series in any sea level comparison is required to have a zero mean. However, by removing the mean of each time series, we also lose information on the mean differences between data sets.

The warm and cold phases of the ENSO are clearly evident in the tide gauge data for the stations in the east and west.

Table 1. Evaluation of Ocean General Circulation Model (OGCM) Simulations of Surface Temperature Forced by Special Sensor Microwave Imager (SSM/I) and European Centre for Medium-Range Weather Forecasts (ECMWF) Winds

	Mean of Deviations From AVHRR	Variance of Deviations From AVHRR	Correlation Coefficient
	140°W		
SSM/I	0.18	0.88	0.78
ECMWF	0.57	1.25	0.67
Significance	0.000	0.001	0.002
	130°W		
SSM/I	−0.14	1.04	0.81
ECMWF	0.76	1.64	0.68
Significance	0.000	0.000	0.000
	110°W		
SSM/I	−0.22	1.50	0.80
ECMWF	1.07	1.78	0.74
Significance	0.000	0.097	0.034

Values are given in degrees Celsius. Errors are computed as deviations of the OGCM simulations from advanced very high resolution radiometer (AVHRR) observations. The means and variances of the errors are listed together with correlation coefficients between simulations and observations. The probability that the difference in errors (or correlation coefficients) occurs by pure chance from data with equal mean, variance, or equal correlations is indicated as "Significance."

During the warm phase in 1987 the deviations are negative in the west and positive in the east, and they reverse after February 1988. For the central Pacific the mean deviation is small (e.g., for the first 2 years at Nauru). If the tide gauge measurements are used as standard, the model simulations perform better in the east and west but not very well at Kanton and Christmas in capturing the cold anomalies for 1988. The Geosat data, on the contrary, capture both the warm and cool phase of ENSO in Kanton and Christmas but not at Santa Cruz. At the Santa Cruz station, tide gauge and model data go from positive to negative almost linearly in 1988, reflecting the transition from the warm to the cool phases of ENSO. However, no such trend is found in Geosat data; the satellite data show a higher sea level than other data for the cool phase of ENSO in the boreal summer and fall of 1988. Unfortunately, there are no altimeter data after February 1989, and the altimeter sampling is quite different from the other three data sets.

In general, the sea level change derived from OGCM and the sea level from the altimeter agree with the tide gauge, as suggested by previous evaluations of Geosat altimeter data in the tropical Pacific using in situ measurements [*Cheney et al.*, 1989; *Wyrtki and Mitchum*, 1990; *Tai et al.*, 1989] and simulated dynamic height [*Chao et al.*, 1993]. The correlation coefficients between model simulations and observations at tide gauges shown in Table 3 are all significant with less than 1% probability that the correlation coefficients arise by pure chance from uncorrelated data. Although the model responses to the SSM/I winds have higher correlation with tide gauge data than the responses to the ECMWF winds, the improvements in correlation are small. The differences in correlation coefficients are obviously insignificant at Nauru and Kanton, and there is slightly less than 20% probability that the improvements at other stations arise by chance.

5.4. Zonal Current

Comparisons of zonal currents at 10-m depth and 100-m depth are presented in Figure 4 for three locations where in situ current measurements are available. Since the buoy data include strong high-frequency variations, a 10-day running mean filter has been applied for clearer display. At both levels the OGCM results from both wind forcing do not agree very well with the results derived from buoy data. The correlation coefficients between current simulations and observations are largely insignificant. The low correlation between model simulation under both winds and observations perhaps reflects measurement problems but is more likely the result of deficiencies in model dynamics. The differences in simulating zonal current between the two wind fields are statistically insignificant.

6. Upper Ocean Heat Budget

In Plate 4 the depth—time variation in model temperature clearly shows that the mixed-layer depth decreases from west to east and the mixed layer is shallow for almost the full year of 1988 and again in the second half of 1989. In 1988 the 20°C isotherm, which has been widely used to locate the bottom of the mixed layer, reaches the surface at 110°W. This is in agreement with the variation of sea surface temperature and steric level shown in Plate 2 and Figure 3. From Plate 4 it is obvious that the difference in the temperature caused by different wind forcing has its maximum below the surface and is likely to result from the different amount of thermocline uplifting.

To understand the difference in temperature responses to the two wind forcings, the heat balance in the upper ocean is examined. The heat balance equation is

$$\frac{\partial T}{\partial t} = -U\frac{\partial T}{\partial x} - V\frac{\partial T}{\partial y} - W\frac{\partial T}{\partial z} + \frac{\partial Q}{c\rho\partial z} + D$$

where T is the temperature, Q is the heat flux, ρ is the density, c is the specific heat, D is transport by turbulent diffusion, and U, V, and W are the zonal, meridional, and vertical component of the current. All the terms in the equation are integrated over a volume of water between the surface and 50 m and bounded by 5°N, 5°S, 140°W, and 110°W. Under both wind forcings the sum of the first four terms on the right side of the equation agrees very closely with the term of the left side (not shown), both in magnitude and in variation, suggesting that the diffusion transport D is negligible. The variations of T averaged over this volume are similar to the variations of SST (not shown). With both wind forcings the surface heat flux and all advection components contribute to the change of heat storage, but the largest terms are the warming by the surface heat flux (positive) and the cooling due to vertical advection (negative); they largely compensate each other. In Plate 5 the difference in responses to the two wind forcings is clearly evident in the difference in $\partial T/\partial t$ and vertical advection, from March to May 1988. During the onset of the 1988 cold phase, SSM/I winds forced a higher thermocline, facilitated a stronger vertical cold advection, and therefore produced a cooler surface temperature.

7. Discussion and Conclusion

The results of this study contribute to three areas. They show that space-based winds are superior to NWP winds in forcing

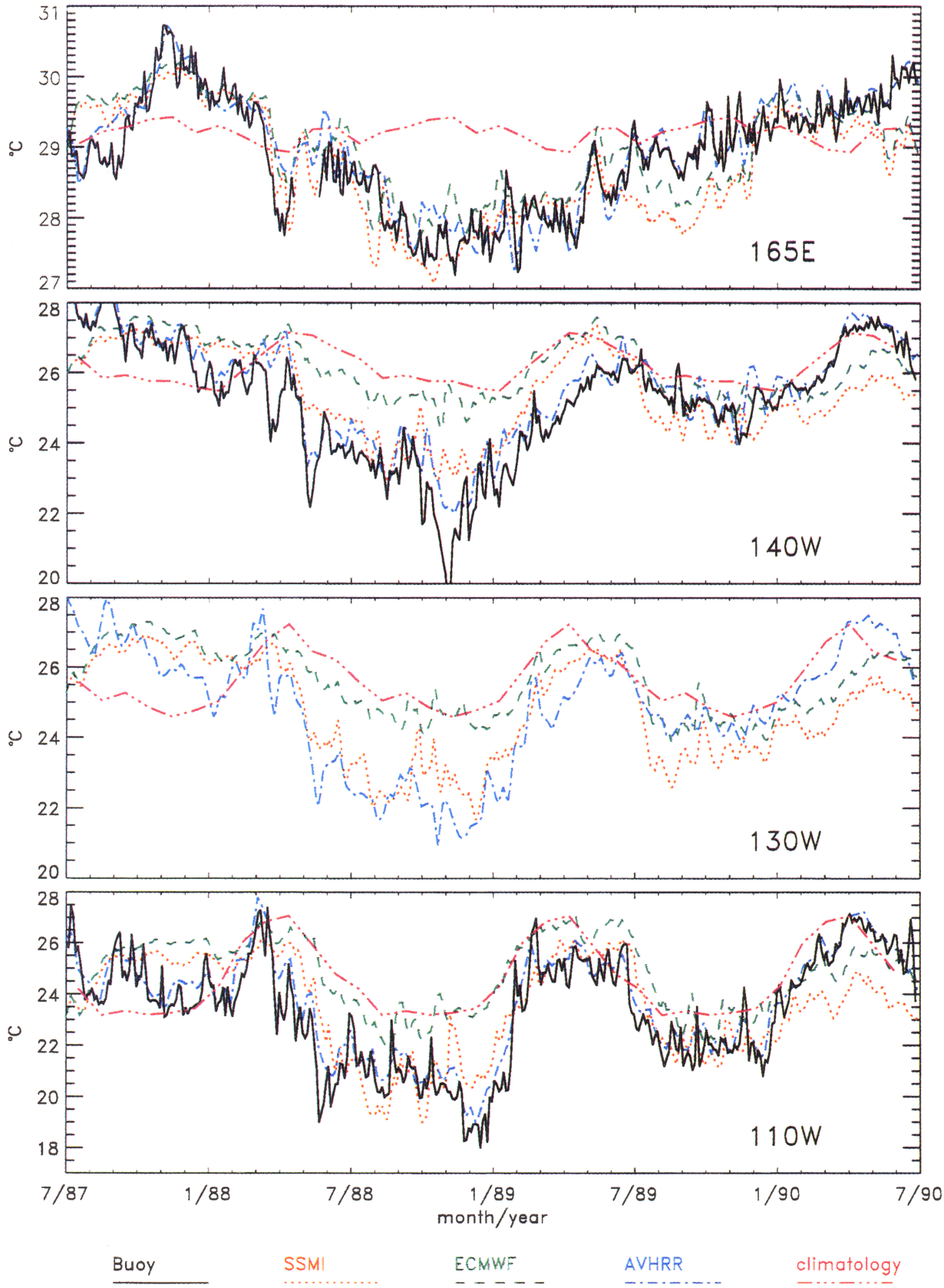

Plate 2. Comparison of first-level (5-m) temperatures produced by the ocean general circulation model (OGCM), when forced by SSM/I and ECMWF winds, with advanced very high resolution radiometer (AVHRR) and buoy sea surface temperatures (SST) at four locations (longitudes are indicated in the plate) along the equator. The climatological annual cycle derived from the AVHRR SST is also shown.

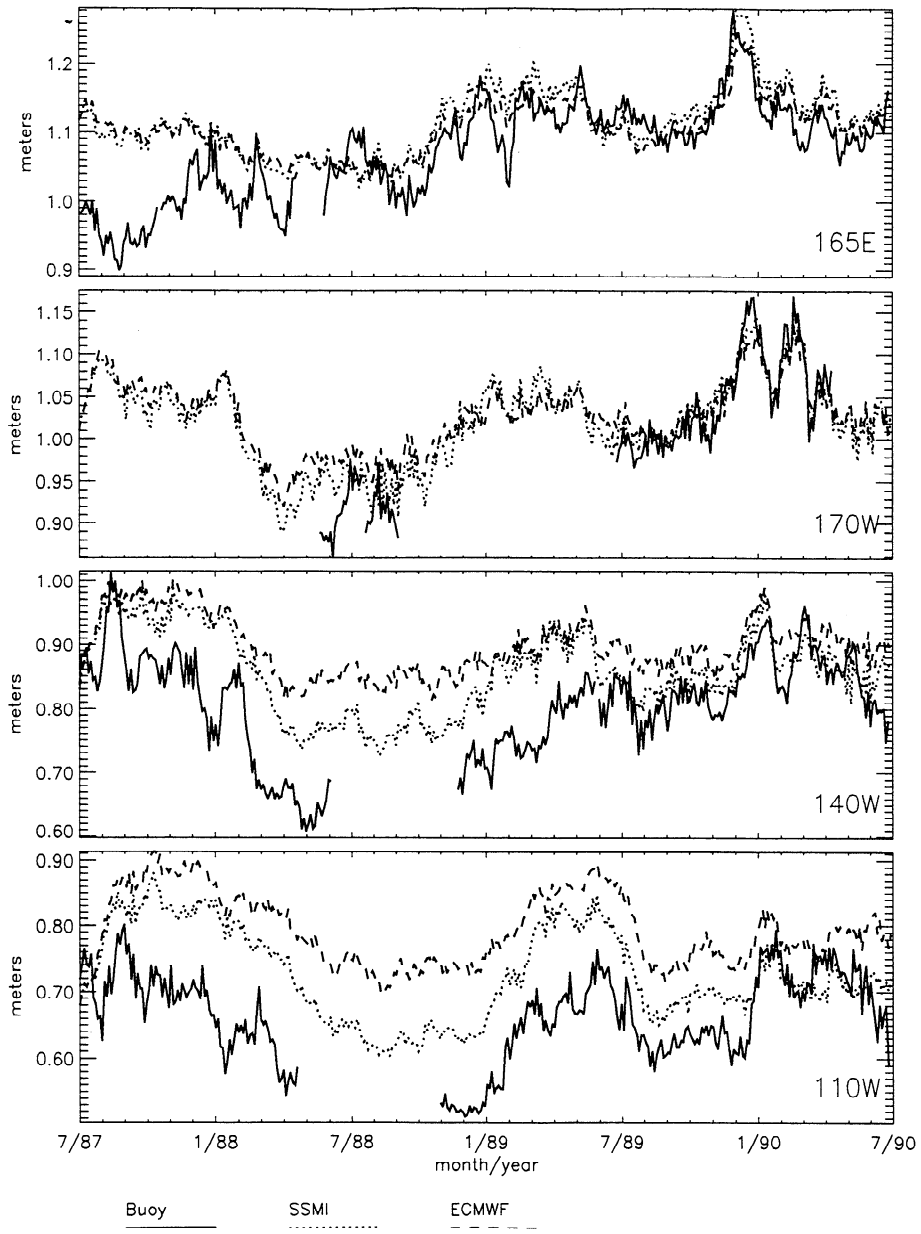

Figure 3. Comparison of steric level (dynamic height) from 300-m depth to the surface, derived from the OGCM density profiles, when forced by SSM/I and ECMWF winds, with buoy measurements at four locations (longitudes are indicated in the figure) along the equator.

realistic oceanic response, infer some deficiencies in the OGCM, and identify the dominant wind-driven mechanism for anomalous upper ocean cooling.

In the past, NWP winds averaged over model grid size and space-based winds averaged over satellite footprint were evaluated largely by direct comparison with coincident in situ measurements at a certain location, but the sparcity of accurate in situ measurement and the neglected spatial variance caused considerable uncertainty. In this study, SSM/I winds are compared with ECMWF winds through the oceanic responses they excited. By comparing OGCM simulations of SST with in situ and space-based observations, we clearly demonstrate that the SSM/I winds generate more realistic anomalous cooling than ECMWF winds. The difference is more than 3°C in the eastern equatorial Pacific during the cool phase of ENSO in 1988. In

Table 2. Same as Table 1, Except for Dynamic Height Instead of Surface Temperature and Buoy Data Instead of AVHRR

	Mean of Deviation From Buoy Data	Variance of Deviation From Buoy Data	Correlation Coefficient
	140°W		
SSM/I	0.067	0.0031	0.71
ECMWF	0.102	0.0033	0.71
Significance	0.000	0.694	0.960
	110°W		
SSM/I	0.081	0.0039	0.54
ECMWF	0.142	0.0040	0.46
Significance	0.000	0.681	0.185

Values are given in meters.

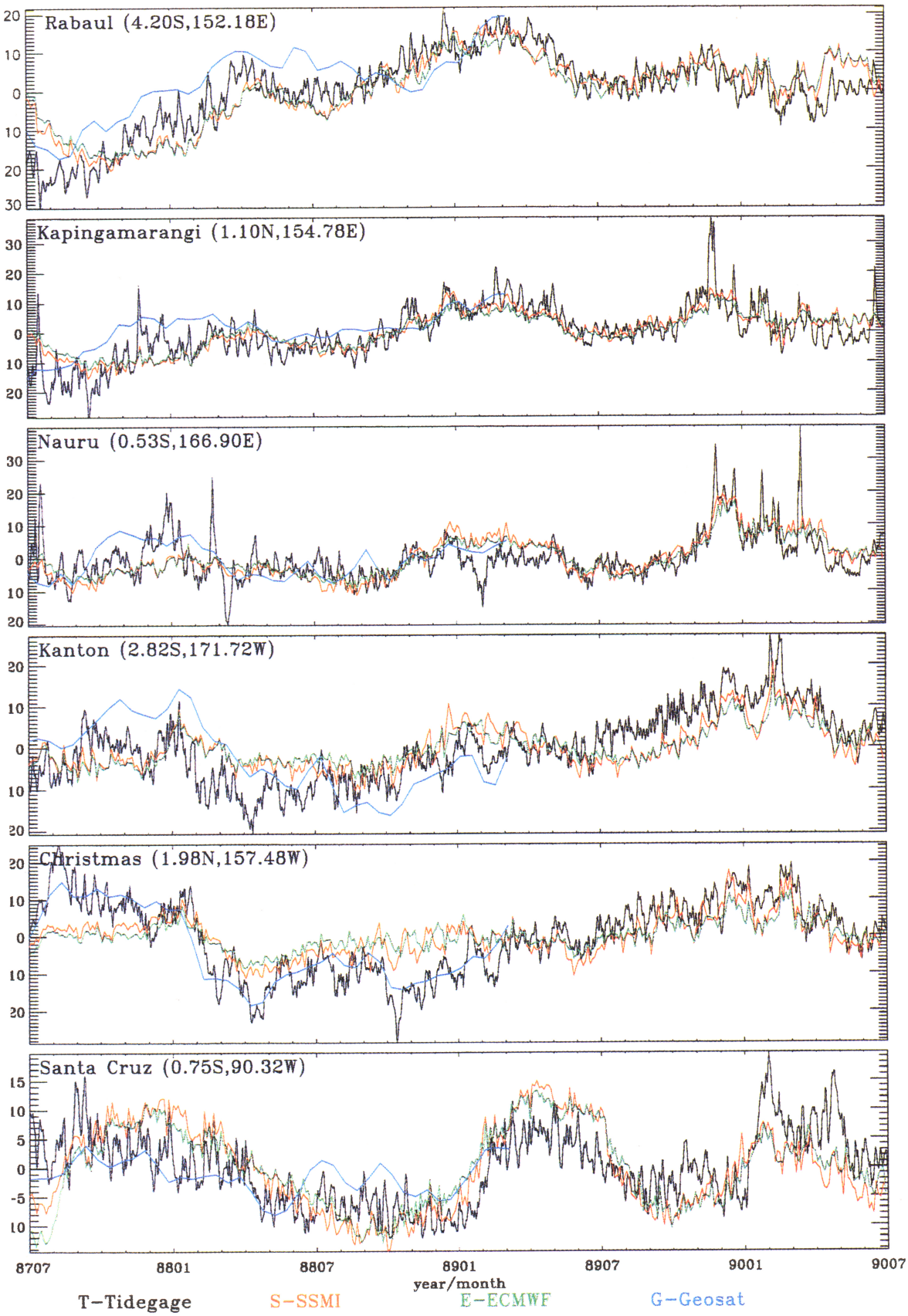

Plate 3. Comparison of sea level change derived from the OGCM, when forced by SSM/I and ECMWF winds, with measurements at tide gauge stations (locations are indicated in the plates) and observations by the Geosat altimeter.

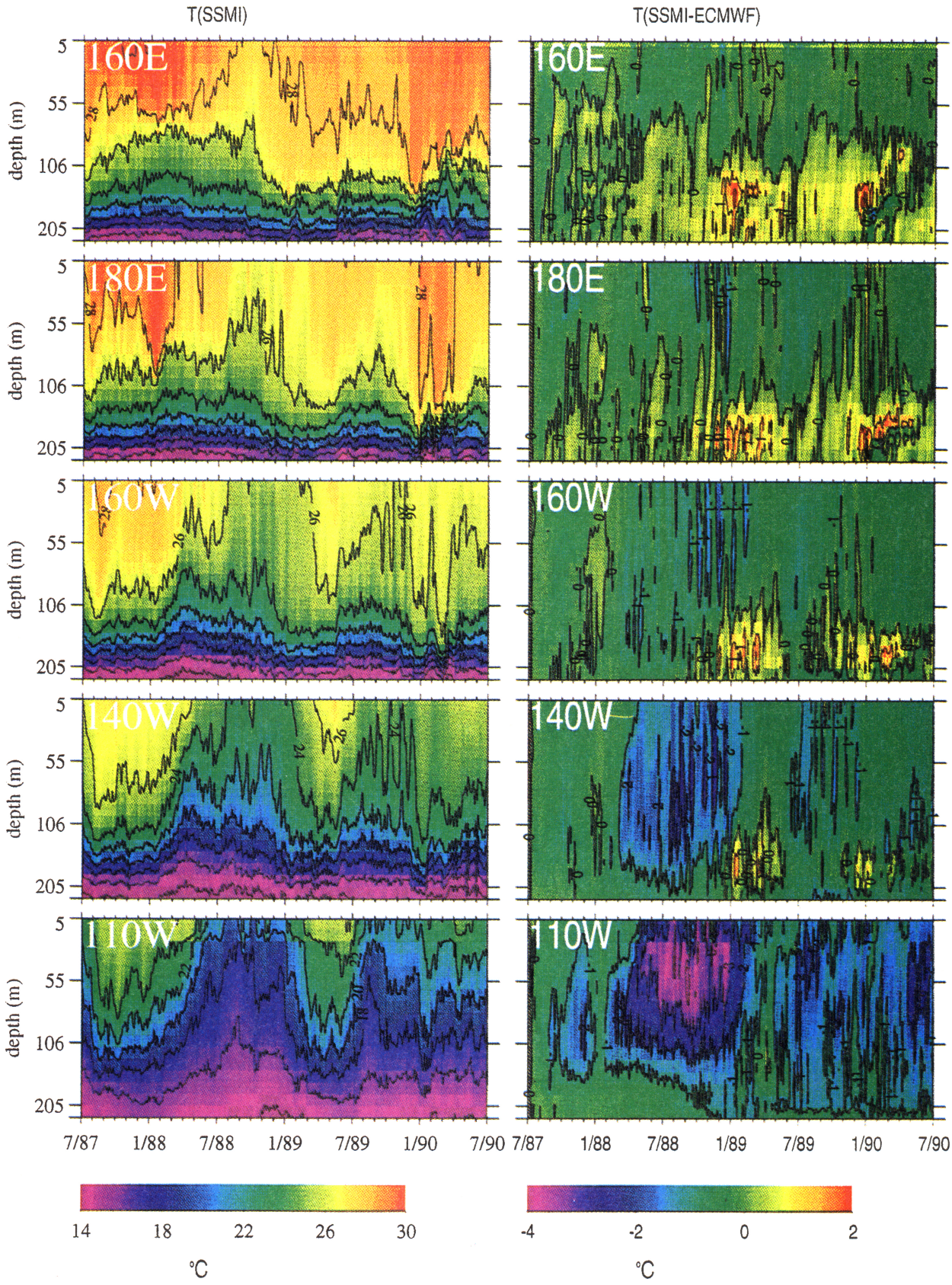

Plate 4. (left) The time–depth variation of temperature from the model driven by SSM/I winds and (right) the time–depth variation of the difference between temperatures from the OGCM driven by SSM/I and ECMWF winds.

Table 3. Correlation Coefficients Between Simulated Sea Level Change and Tide Gauge Observations

Station	SSM/I	ECMWF	Significance
Rabaul	0.83	0.79	0.16
Kapingamarangi	0.78	0.75	0.29
Nauru	0.63	0.62	0.96
Kanton	0.67	0.66	0.84
Christmas	0.71	0.66	0.17
Santa Cruz	0.61	0.54	0.19

The probability that the difference in the coefficients arises by chance from equal values is listed under "Significance."

the same area and for the same time period, SSM/I winds force a lower steric level, showing the depth-integrated effect of different winds. The steric changes should follow temperature change and affect sea level. However, mean difference in sea level caused by wind forcing cannot be examined because the mean sea level has to be removed before comparison.

Since model surface temperature, steric height, and sea level, resulting from both wind forcings, correlate significantly with observations, the OGCM appears to be robust in simulating the temporal variation of thermal (or steric) quantities. This is in contrast with the simulation of ocean current. The

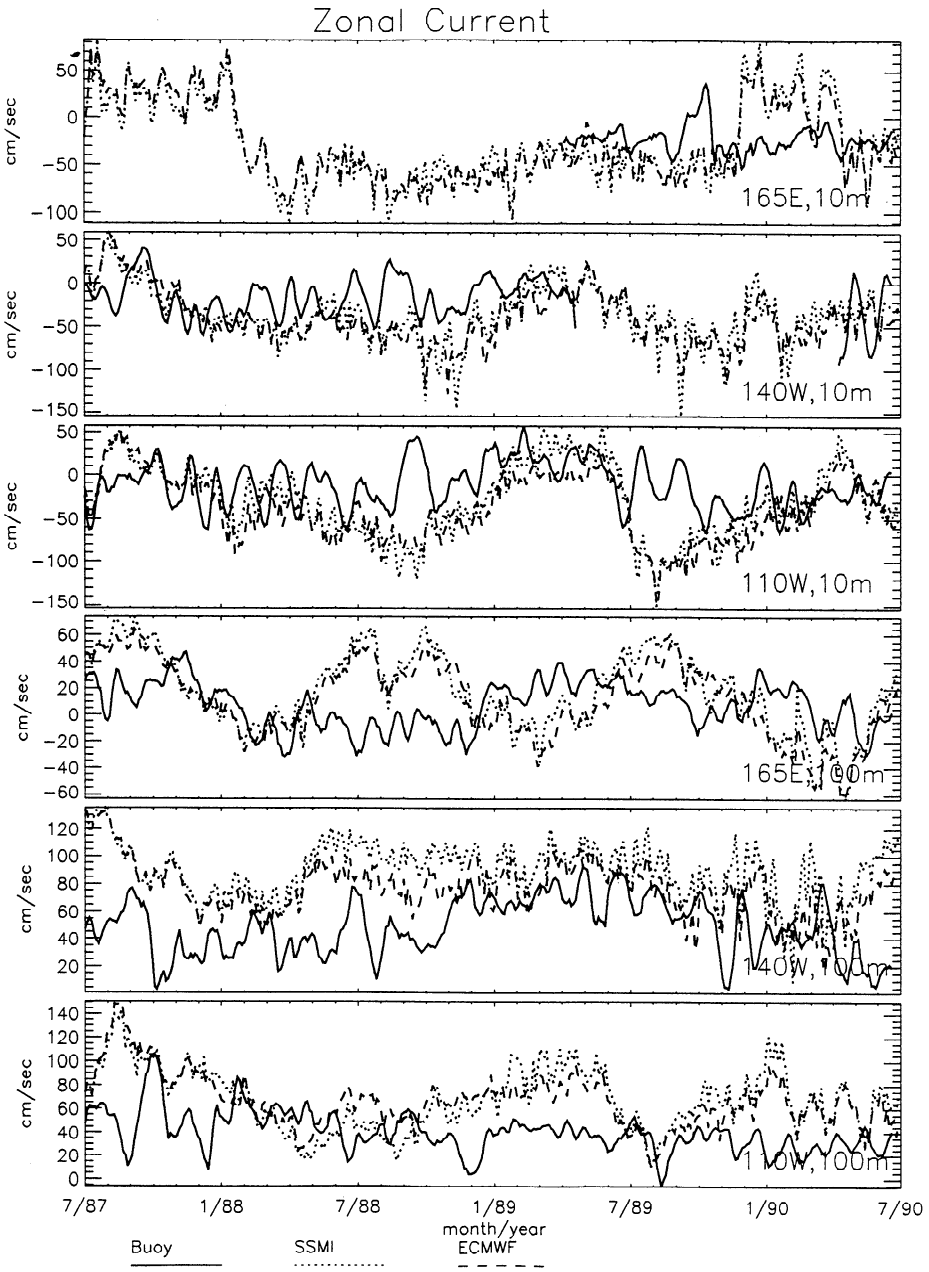

Figure 4. Comparison of the zonal components of the surface current at two depths derived from the OGCM, when forced by SSM/I and ECMWF winds, with buoy measurements at three locations (the depths and longitudes are indicated in the figures) along the equator. A 10-day running mean filter has been applied for graphic clarity.

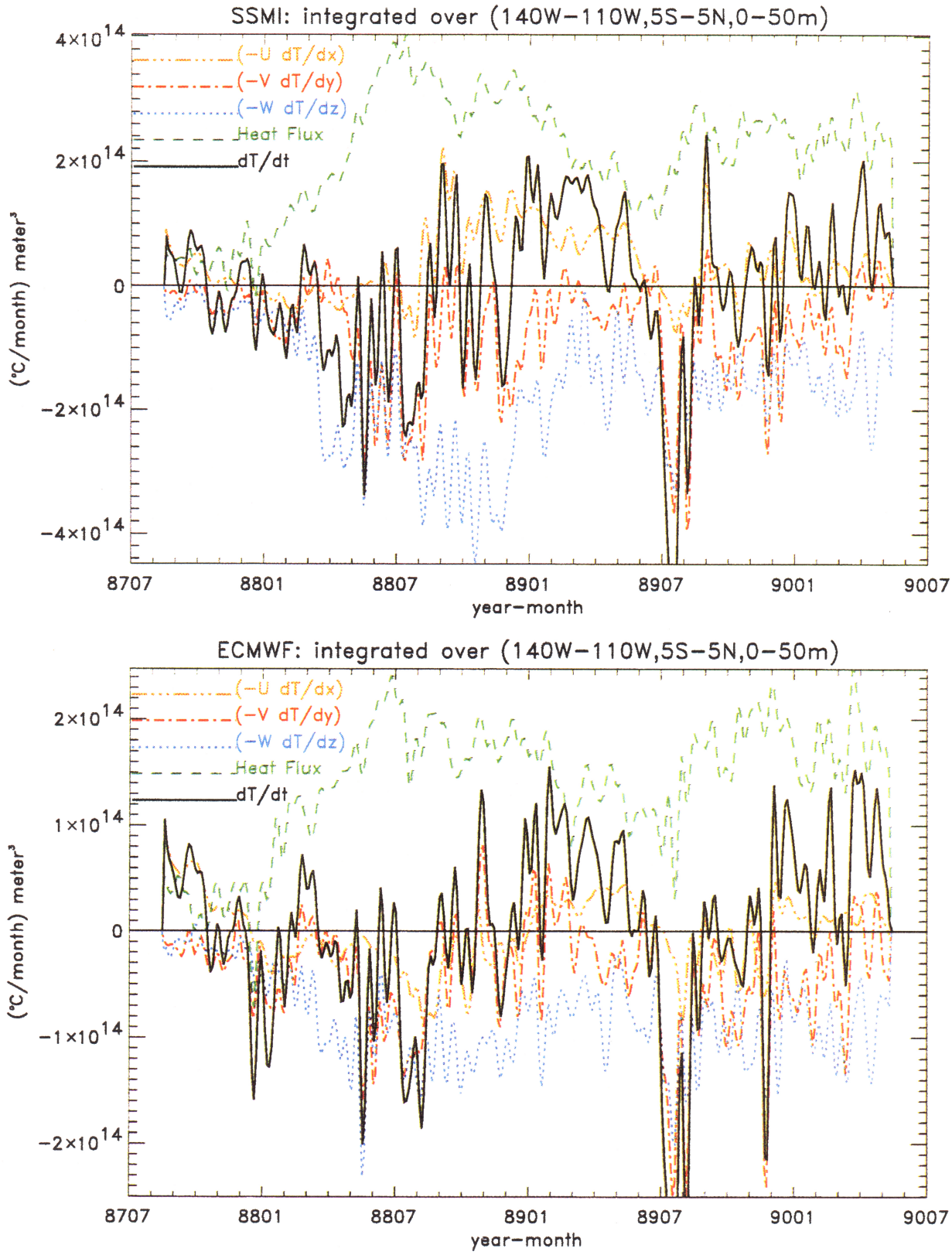

Plate 5. Ocean heat budget components simulated by the OGCM when forced by (top) SSM/I and (bottom) ECMWF winds, averaged over the volume between the surface and 50-m depth, within 5° latitude from the equator, and bounded by longitudes 110°W and 140°W. The components are heat storage change, surface heat flux, zonal advection, meridional advection, and vertical advection.

temporal variations of zonal current simulated with both wind forcings differ from the variation of current measurement at the mooring; no significant correlation is found between simulations and observations. Past studies on the qualitative behavior or the temporal mean of the simulated currents [e.g., *Philander et al.*, 1987; *Halpern et al.*, 1995] appear to cast a more optimistic view of the capability of the OGCM in simulating ocean currents. There are discrepancies between model simulations of other parameters and observations too. For example, both wind fields produce unrealistic cold anomalies in first half of 1990, particularly in the eastern equatorial Pacific, and higher steric height in the second half of 1987. Discrepancies between model simulations and observations, common to both wind forcings, found in this study infer deficiencies in the OGCM physics.

The OGCM provides simulation of wind-driven heat advection in the ocean mixed layer which is hidden from spaceborne sensors and which cannot be adequately resolved by in situ observations. Previous studies on upper ocean heat balance in the eastern Pacific, whether from climatological data [e.g., *Wyrkti*, 1981; *Enfield*, 1986] or from model simulations forced by climatological fluxes [e.g., *Philander et al.*, 1987; *Seager et al.*, 1988], are largely confined to seasonal variations. The results from this study clearly demonstrate that differences in SST simulations for the two wind forcings are largely caused by different degrees of thermocline uplifting and vertical heat advection. The inference is that mixed-layer depth and vertical advection are the dominant wind-driven factors for anomalous SST changes. Significant differences in zonal wind stress are found off-equator, while significant differences in temperature are more confined to the equator and coastal regions, demonstrating that forcing and response are largely remotely connected.

Since the main variable in forcing the OGCM is the wind stress, we simply imitated traditional methods of applying surface thermal forcing for this OGCM [e.g., *Philander et al.*, 1987; *Chao et al.*, 1993]; the OGCM might have been tuned to these types of thermal forcing. There is no temporal variation in the radiative fluxes, and there is no interannual variation in the air temperature and humidity which control the turbulent heat fluxes. The transfer coefficients used for sensible and latent heat fluxes are not the most up to date. In simple test cases we conducted, changing the method of computing the heat flux only changed the SST by a similar amount in both runs but could not eliminate the large difference in the thermal fields created by the two wind forcings. In computing the significance of the mean, variance, and correlation, the data in the ensemble are assumed to be independent which may also be erroneous.

This study demonstrates the historical opportunity offered by the availability of an array of spaceborne ocean sensors, the establishment of in situ monitoring systems by TOGA, and the maturity of ocean general circulation models [*Liu et al.*, 1995]. Together with the advance of computer technology that makes available affordable computer power to run the OGCM and analyze the large amount of satellite data, they are a set of powerful tools for understanding atmospheric forcing and oceanic response in the near future.

Acknowledgments. This study was performed at the Jet Propulsion Laboratory, California Institute of Technology, under contract with the National Aeronautics and Space Administration (NASA). The SSM/I wind field was produced at the NASA Goddard Space Flight Center. We are grateful to Victor Zlotnicki for his version of the Geosat sea level. This study was supported by the NASA Scatterometer Project, the Topex/Poseidon Project, and the Earth Observing System Interdisciplinary Science Investigation.

References

Atlas, R., S. C. Bloom, R. N. Hoffman, J. Ardizzone, and G. Brin, Space-based surface wind vectors to aid understanding of air-sea interactions, *Eos Trans. AGU, 72*, 201, 204–205, 208, 1991.

Atlas, R., R. N. Hoffman, and S. C. Bloom, Surface wind velocity over the ocean, in *Atlas of Satellite Observations Related to Global Changes*, edited by R. J. Gurney, J. L. Foster, and C. L. Parkinson, pp. 129–139, Cambridge Univ. Press, New York, 1993.

Bengtsson, L., M. Kanamitsu, P. Kallberg, and S. Uppala, FGGE 4-dimensional data assimilation at ECMWF, *Bull. Am. Meteorol. Soc., 63*, 29–43, 1982.

Bryan, K., and M. D. Cox, An approximate equation of state for numerical models of ocean circulation, *J. Phys. Oceanogr., 2*, 510–514, 1972.

Bunker, A. F., Computations of surface energy flux and annual air-sea interaction cycles of the North Atlantic Ocean, *Mon. Weather Rev., 104*, 1122–1140, 1976.

Busalacchi, A. J., R. M. Atlas, and E. C. Hackert, Comparison of special sensor microwave imager vector wind stress with model-derived and subjective products for the tropical Pacific, *J. Geophys. Res., 98*, 6961–6977, 1993.

Chao, Y., D. Halpern, and C. Perigaud, Sea surface height variability during 1986–1988 in the tropical Pacific Ocean, *J. Geophys. Res., 98*, 6947–6959, 1993.

Cheney, R. E., B. C. Douglas, R. W. Agreen, L. Miller, and D. L. Porter, Geosat Altimeter Geophysical Data Record User Handbook, *NOAA Tech. Memo. NOS NGS-46*, 20 pp., Natl. Geod. Surv., Rockville, Md., 1987.

Cheney, R. E., B. C. Douglas, and L. Miller, Evaluation of Geosat altimeter data with application to tropical Pacific sea level variability, *J. Geophys. Res., 94*, 4737–4747, 1989.

Enfield, D. B., Zonal and seasonal variation of the near-surface heat balance of the equatorial Pacific Ocean, *J. Phys. Oceanogr., 16*, 1038–1054, 1986.

Gill, A. E., and P. P. Niiler, The theory of the seasonal variability in the ocean, *Deep Sea Res., 20*, 141–177, 1973.

Halpern, D., A. Hollingsworth, and F. Wentz, ECMWF and SSM/I global surface wind speeds, *J. Atmos. Oceanic Technol., 11*, 779–788, 1994.

Halpern, D., Y. Chao, C. C. Ma, and C. R. Mechoso, Comparison of tropical temperature and current simulations with two ertical mixing schemes embedded in an ocean general circulation model and reference to observations, *J. Geophys. Res., 100*, 2515–2522, 1995.

Hayes, S. P., L. J. Mangum, J. Picaut, A. Sumi, and K. Takeuchi, TOGA-TAO: A moored array for real-time measurements in the tropical Pacific Ocean, *Bull. Am. Meteorol. Soc., 72*, 339–347, 1991.

Hellerman, S., and M. Rosenstein, Normal monthly wind stress over the world ocean with error estimates, *J. Phys. Oceanogr., 13*, 1093–1104, 1983.

Levitus, S., Climatological Atlas of the World Ocean, *NOAA Prof. Pap. 13*, 173 pp., Natl. Oceanic and Atmos. Admin., Silver Spring, Md., 1982.

Liu, W. T., K. B. Katsaros, and J. A. Businger, Bulk parameterization of air-sea exchange in heat and water vapor including the molecular constraints at the interface, *J. Atmos. Sci., 36*, 1722–1735, 1979.

Liu, W. T., W. Tang, and L. L. Fu, Recent warming event in the Pacific may be an El Niño, *Eos Trans. AGU, 76*, 429, 437, 1995.

McPhaden, M. J., and S. Hayes, Variability in the eastern equatorial Pacific Ocean during 1986–1988, *J. Geophys. Res., 95*, 13,195–13,208, 1990.

Oort, A. H., Y. H. Pan, R. W. Reynolds, and C. F. Ropelewski, Historical trends in the surface temperature over the oceans based on the COADS, *Clim. Dyn., 2*, 29–38, 1987.

Philander, S. G. H., W. J. Hurlin, and A. D. Seigel, A model of the seasonal cycle in the tropical Pacific Ocean, *J. Phys. Oceanogr., 17*, 1986–2002, 1987.

Press, W. H., B. P. Flannery, S. A. Teukolsky, and W. T. Vetterling, *Numerical Recipes*, p. 465, Cambridge Univ. Press, New York, 1989.

Reynolds, R. W., and T. M. Smith, Improved global sea surface temperature analyses using optimum interpolation, *J. Clim., 7*, 929–948, 1994.

Seager, R., S. E. Zebiak, and M. A. Cane, A model of the tropical Pacific sea surface temperature climatology, *J. Geophys. Res.*, *93*, 1265–1280, 1988.

Tai, C. K., W. B. White, and S. E. Pazan, Geosat crossover analysis in the tropical Pacific, 2, Verification analysis of altimetric sea level maps with expendable bathythermograph and island sea level data, *J. Geophys. Res.*, *94*, 897–908, 1989.

Tang, W., and W. T. Liu, The Pacific responses exhibited by an OGCM to various wind fields, in *PORSEC-'92*, pp. 408–413, PORSEC Secr. Publ., Shimizu, Japan, 1992.

Wentz, F. J., Measurement of oceanic wind vectors using satellite microwave radiometer, *IEEE Trans. Geosci. Remote Sens.*, *30*, 960–972, 1992.

Wyrtki, K., An estimate of equatorial upwelling in the Pacific, *J. Phys. Oceanogr.*, *11*, 1205–1214, 1981.

Wyrtki, K., and G. Mitchum, Interannual difference of Geosat altimeter heights and sea level: The importance of a datum, *J. Geophys. Res.*, *95*, 2969–2975, 1990.

Wyrtki, K., K. Constantine, B. Kilonsky, G. Mitchum, B. Miyamoto, T. Murphy, and S. Nakahar, The Pacific Island Sea Level Network, *JIMAR Data Rep. 002*, 71 pp., Univ. of Hawaii, Honolulu, 1988.

Zlotnicki, V., L. L. Fu, and W. Patzert, Seasonal variability in global sea level observed with Geosat altimetry, *J. Geophys. Res.*, *94*, 17,959–17,969, 1989.

R. Atlas, Laboratory for Atmospheres, NASA Goddard Space Flight Center, Greenbelt, MD 20771.

W. T. Liu and W. Tang, Jet Propulsion Laboratory, California Institute of Technology, 4800 Oak Grove Drive, Pasadena, CA 91109. (e-mail: liu@pacific.jpl.nasa.gov)

(Received May 9, 1995; revised March 15, 1996;
accepted April 29, 1996.)